Transverse collapse of low-frequency Alfvén waves

D. Laveder[1], T. Passot and P.L. Sulem

CNRS UMR 6529, Observatoire de la Côte d'Azur,
BP 4229, 06304 Nice Cedex 4, France

Abstract

The dynamics of long-wavelength dispersive Alfvén wave trains propagating parallel to an ambient field in a magnetized plasma is investigated by means of a three-dimensional extension of the derivative nonlinear Schrödinger equation that includes the mean effect of the longitudinal magneto-sonic waves.

In the strongly dispersive regime, quasi-monochromatic right-hand polarized plane waves perturbed by a broad-spectrum noise develop a transverse collapse leading to the formation of strong magnetic filaments parallel to the ambient field, as asymptotically predicted by the nonlinear Schrödinger equation for the wave envelope. In contrast, for left-hand polarized waves filamentation only takes place when the noise is confined to Fourier modes with wavenumbers close enough to that of the pump.

In the regime where dispersion and nonlinearity are comparable, the amplitude growth is strongly inhibited but intense gradients are still formed, associated with the creation of pancake-like magnetic structures.

The transverse focusing of weakly-nonlinear dispersive waves still takes place when the spectrum of the initial conditions is broadened, in spite of the fragmentation of the magnetic filaments into chains of magnetic bubbles and ultimately into randomly distributed three-dimensional structures.

Key words: Alfvén waves, wave collapse, filamentation, Derivative Nonlinear Schrödinger Equation
PACS numbers: 52.35 Bj, 52.35 Mw, 52.65.Kj, 95.30.Qd.

[1] corresponding author. E-mail: laveder@obs-nice.fr

1 Introduction

Hall-MHD, that extends the usual magnetohydrodynamics by retaining the effect of ion inertia in a generalized Ohm's law, provides a good description of magnetized plasmas at large to intermediate scales, when kinetic effects are neglected [1]. It is also an interesting paradigm of a system where dispersive waves coexist with hydrodynamic phenomena. The equations read

$$\partial_t \rho + \nabla \cdot (\rho \mathbf{u}) = 0 \tag{1}$$

$$\rho(\partial_t \mathbf{u} + \mathbf{u} \cdot \nabla \mathbf{u}) = -\frac{\beta}{\gamma} \nabla \rho^\gamma + (\nabla \times \mathbf{b}) \times \mathbf{b} \tag{2}$$

$$\partial_t \mathbf{b} - \nabla \times (\mathbf{u} \times \mathbf{b}) = -\frac{1}{R_i} \nabla \times \Big(\frac{1}{\rho} (\nabla \times \mathbf{b}) \times \mathbf{b} \Big) \tag{3}$$

$$\nabla \cdot \mathbf{b} = 0. \tag{4}$$

As usual, ρ is the density of the plasma, $\mathbf{u}$ its velocity and $\mathbf{b}$ the magnetic field. The equations are written in a non-dimensional form, taking as unity the Alfvén speed $c_A = B_0/\sqrt{4\pi\rho_0}$, where B_0 is the magnitude of a reference magnetic field and ρ_0 the mean density of the plasma. The parameter $\beta = c_s^2/c_A^2$, where c_s is the sound velocity, measures the relative importance of the thermal and magnetic pressures, γ is the polytropic gas constant and R_i denotes the non-dimensional ion-cyclotron frequency.

In the presence of an ambient magnetic field, an important phenomenon is the propagation of Alfvén waves, corresponding to transverse oscillations of the magnetic field lines. These waves are believed to play a significant role in space plasmas since they can propagate over large distances without being dissipated [2], [3]. Assuming $\beta \neq 1$, the Alfvén wave dynamics can be isolated when concentrating on wavelengths much larger than the ion-inertial length. Through a usual reductive perturbative expansion, waves propagating parallel or quasi-parallel to the ambient magnetic field are then described, when restricted to be one-dimensional, by the so-called derivative nonlinear Schrödinger equation (DNLS) [4]–[8]

$$\partial_\tau b + \frac{1}{4(1-\beta)} \partial_\xi \Big((|b|^2 - \langle |b|^2 \rangle) b \Big) + \frac{i}{2R_i} \partial_{\xi\xi} b = 0, \tag{5}$$

a soliton equation integrable by inverse scattering [9]. In eq. (5), the background magnetic field points in the x-direction, the transverse magnetic field b stands for the complex field $b_y + i b_z$ rescaled by the wave magnitude $\epsilon^{1/2}$. The stretched variables are defined as $\xi = \epsilon(x - t)$ and $\tau = \epsilon^2 t$. Brackets indicate averaging along the direction of propagation.

The three-dimensional equations governing the evolution of localized waves when transverse variations on scales $\eta = \epsilon^{3/2}y$, $\zeta = \epsilon^{3/2}z$ are allowed, are given in [10]. They have to be generalized in the case of modulated wave trains by retaining mean fields resulting from the averaging of magneto-sonic waves along the direction of propagation [11], which leads to the three-dimensional DNLS equations (3D-DNLS) [12]

$$\partial_\tau b + \partial_\xi \left(\frac{1}{2}bP + (\bar{u}_x + \frac{1}{2}\bar{b}_x)b\right) - \frac{1}{2}\partial_\perp P + \frac{i}{2R_i}\partial_{\xi\xi} b = 0 \tag{6}$$

$$\partial_\tau \bar{u}_x = \frac{1}{2}\left(\partial_\perp^* \langle bP\rangle + \partial_\perp \langle b^* P\rangle\right) \tag{7}$$

$$\partial_\xi \widetilde{b}_x + \frac{1}{2}\left(\partial_\perp^* b + \partial_\perp b^*\right) = 0. \tag{8}$$

In the above equations, bars or brackets $\langle\cdot\rangle$ indicate averages over the ξ-variable and the notation $\partial_\perp = \partial_\eta + i\partial_\zeta$ has been introduced. The induced longitudinal magnetic field that like the mean longitudinal velocity $\bar{u}_x$ is rescaled by a factor ϵ, is separated in mean and fluctuating part in the form $\bar{b}_x + \tilde{b}_x$. Furthermore, $\bar{b}_x = \frac{1}{1+\beta}(-\frac{\langle|b|^2\rangle}{2} + E_M)$ where the constant E_M, defined as the average over the whole domain of the magnetic energy density $\frac{|b|^2}{2}$, is retained to ensure that $\bar{b}_x$ is zero in one space dimension. The fluctuations of magnetic pressure are given by $P = \frac{1}{2(1-\beta)}(2\widetilde{b}_x + |b|^2 - \langle|b|^2\rangle)$.

It is convenient to introduce a parameter ν, representing the relative magnitude of the dispersion and the nonlinearity. For this purpose, denoting by b_0 and k_0^{-1} the initial typical amplitude and longitudinal wavelength of the transverse magnetic field, we rescale b by b_0, the longitudinal and transverse coordinates by k_0^{-1} and $(b_0 k_0)^{-1}$ respectively, the time by $(k_0 b_0^2)^{-1}$, the fields $\bar{u}_x$, $\bar{b}_x$ and $\widetilde{b}_x$ by b_0^2. Equations (7)–(8) then retain the same form, while in eq. (6) the coefficient $\frac{1}{2R_i}$ is replaced by $\nu = \frac{k_0}{2R_i b_0^2}$.

The 3D-DNLS equations provide a considerable simplification of the primitive Hall-MHD equations by concentrating on parallel Alfvén waves propagating in only one direction and by averaging over the magneto-sonic waves. They are in particular well adapted to plasmas with $\beta > 1$ where the decay instability, which requires counter-propagating waves, is absent [13]–[15].

A main phenomenon is the transverse collapse of a slightly perturbed small-amplitude Alfvén wave train (large ν), often referred to as wave filamentation. A simple description is provided by the focusing two-dimensional nonlinear Schrödinger (NLS) equation [16],[17]. In this formalism, the collapse corresponds to a finite-time blowup of the wave amplitude, associated with a breakdown of the modulational description [18]. Wave collapse is a basic mechanism for small-scale formation and plasma heating that for example was extensively studied in the context of Langmuir waves [19].

Several questions are conveniently addressed in the framework of the 3D-DNLS equations. Among them are the domain of validity of the NLS description and the analysis of phenomena occurring for larger wave amplitudes, (moderate or small ν). These issues are here studied by means of numerical integrations of the 3D-DNLS equations with periodic boundary conditions, using a Fourier spectral method. The time stepping is performed with an Adams-Bashford scheme for the nonlinear terms, the dispersion being treated exactly. Comparisons with the predictions of an amplitude model for moderate ν [21],[22] are also presented. Furthermore, the evolution of transversally perturbed wave packets with various spectral width is simulated.

2 Evolution of a perturbed circularly polarized Alfvén wave

2.1 Numerical simulations

The 3D-DNLS equations, like the original Hall-MHD equations, admit exact solutions, named after Ferraro [20], in the form of finite amplitude circularly polarized monochromatic plane waves $b = b_0 e^{-i\sigma(k\xi - \omega\tau)}$ with $\bar{u}_x = 0$, where, choosing $k > 0$, one has $\sigma = 1$ for right-hand and $\sigma = -1$ for left-hand polarization, with a dispersion relation $\omega = \frac{\sigma k^2}{2R_i}$.

As already mentioned, we concentrate on plasmas with $\beta > 1$ where no decay instability is present in the primitive Hall-MHD equations. The dynamics resulting from long-wavelength longitudinal perturbations of a Ferraro wave is for any ν amenable to a modulation analysis using a formalism adapted to finite-amplitude waves [23],[24]. It is then easily seen that a left-hand polarized wave is always stable, while a right-hand polarized wave is unstable when $\nu > \frac{1}{8(\beta-1)}$ and stable otherwise. A direct linear stability analysis is also presented in [15]. For example, for $\beta = 3$, $R_i = 1$, $k = 1$ and $b_0 = 1$, corresponding to $\nu = 0.5$, the growth rate reaches its maximum $\gamma_L \approx 0.1$ (in the primitive DNLS units), at a wavenumber K such that $K/k \approx 0.5$. Whatever their polarizations, Ferraro waves are also unstable to perturbations in the transverse directions: the most unstable transverse mode is of order kb_0 and the growth rate γ_T proportional to kb_0^2 with a coefficient of order unity. For the above parameters, $\gamma_T \approx 1.0$.

In order to address the possible oblique instabilities (not necessarily of modulation type), we performed short-time simulations of eqs. (6)–(8) starting with a circularly polarized wave of unit amplitude and wavenumber $k = 1$ in a $(16\pi) \times (2\pi)^2$-periodic domain, subject to a random noise with Fourier modes of maximum amplitude 10^{-7} covering the whole spectral range of the simulation. For simplicity, the linear study is performed in two space dimensions.

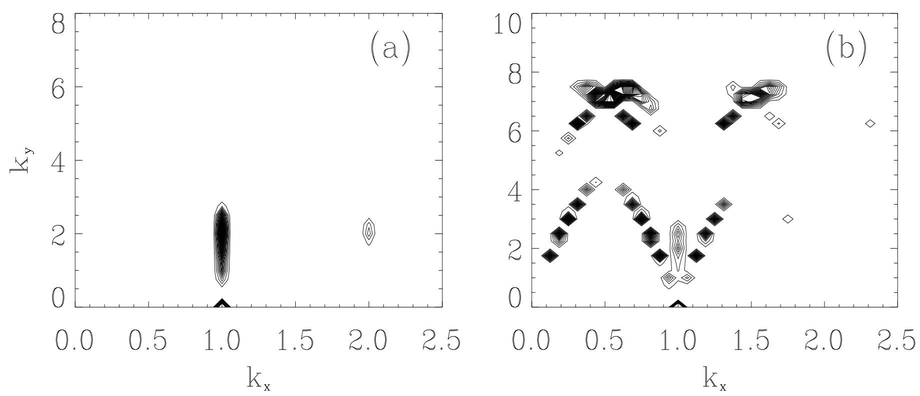

Fig. 1. Spectral instability range as delimited by the contours of Fourier modes of b_y obtained by two-dimensional numerical simulations of the 3D-DNLS equations, for initially right-hand (a) and left-hand (b) circularly polarized Alfvén waves with $\beta = 2$ and $\nu = 50$. The mode $k_x = 1$, $k_y = 0$ corresponds to the pump wave. At the resolution of Fig. 1a, the longitudinal instability is not visible.

We observe that for right-hand polarization, no small-scale oblique instability develops whatever the magnitude of ν. Furthermore, as already known, the longitudinal instability is subdominant. Such a regime is illustrated in Fig. 1a that displays the unstable Fourier modes for $\beta = 2$ and $\nu = 50$. On the other hand, in the case of a left-hand polarized pump, oblique instabilities are present in the large-ν regime (Fig. 1b), with a growth rate that is progressively weakened as the dispersion is reduced and becomes negligible for $\nu = 0.5$.

The nonlinear development of the transverse instability of a small-amplitude pump (large ν) is expected to lead to wave filamentation. This phenomenon is demonstrated by integrating the DNLS equations with initial conditions corresponding to a weakly perturbed right-hand polarized Alfvén wave with $\nu = 50$, in a periodic box whose longitudinal size equals 8 pump wavelengths. The initial random noise has a maximum amplitude of 10^{-7} and affects all the modes present in the simulation. The formation of intense magnetic filaments, where at the end of the simulation the magnetic intensity has been amplified by a factor close to 50, is shown in Fig. 2a.

In the case of left-hand polarization again with $\nu = 50$, a simulation with a broad-spectrum initial noise leads to a regime where small scales are randomly distributed in the whole domain, without any significant amplification of the transverse magnetic field (Fig. 2b). Such a dynamics results from the development of oblique instabilities that dominate over the filamentation. In this regime, filamentation can occur only when the initial noise spectrum is localized near the pump wavevector.

The simulation reported in Fig. 2a shows that subharmonics do not develop

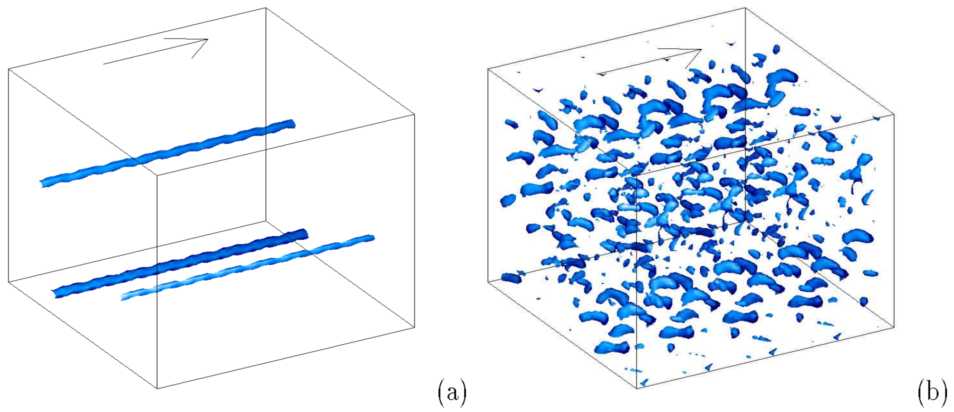

Fig. 2. Isosurfaces $|b|^2 = 20$ for an initially right-hand polarized Alfvén wave (a), and $|b|^2 = 3$ for a left-hand polarized Alfvén wave (b), when $\beta = 2$ and $\nu = 50$. The arrow indicates the direction of the ambient field.

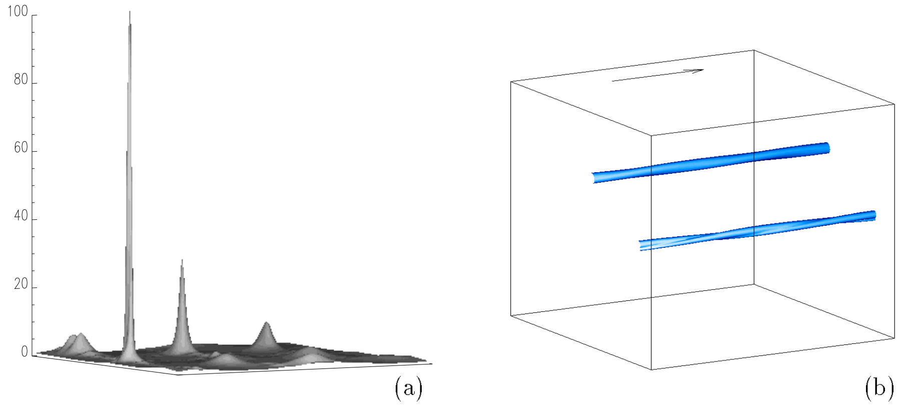

Fig. 3. Snapshot of $|b|^2$ in a plane transverse to the ambient field (a) and three-dimensional isosurfaces $|b|^2 = 10$ (the arrow indicating the direction of the ambient field) (b), for an initially circularly polarized Alfvén wave with $\beta = 3$ and $\nu = 50$ at $t = 9.8$.

during the evolution of a right-hand polarized wave. For a detailed study of the filamentation, we thus choose a right-hand circularly polarized pump with wavenumber $k = 1$ and $\beta = 3$ in a box of size $(2\pi)^3$. We consider three different values of the parameter ν associated with regimes that are strongly ($\nu = 50$), moderately ($\nu = 0.5$) and weakly ($\nu = 0.01$) dispersive. The maximum resolution achieved in these computations is limited to 32×256^2, due to the very small time steps required to prevent numerical instabilities at small scales. In these simulations, the noise is purely transverse and confined to large-scale Fourier modes.

Figure 3a displays a snapshot of the Alfvén wave intensity $|b|^2$ in a plane transverse to the ambient field, for a run with $\nu = 50$, at $\tau = 9.8$. At this time

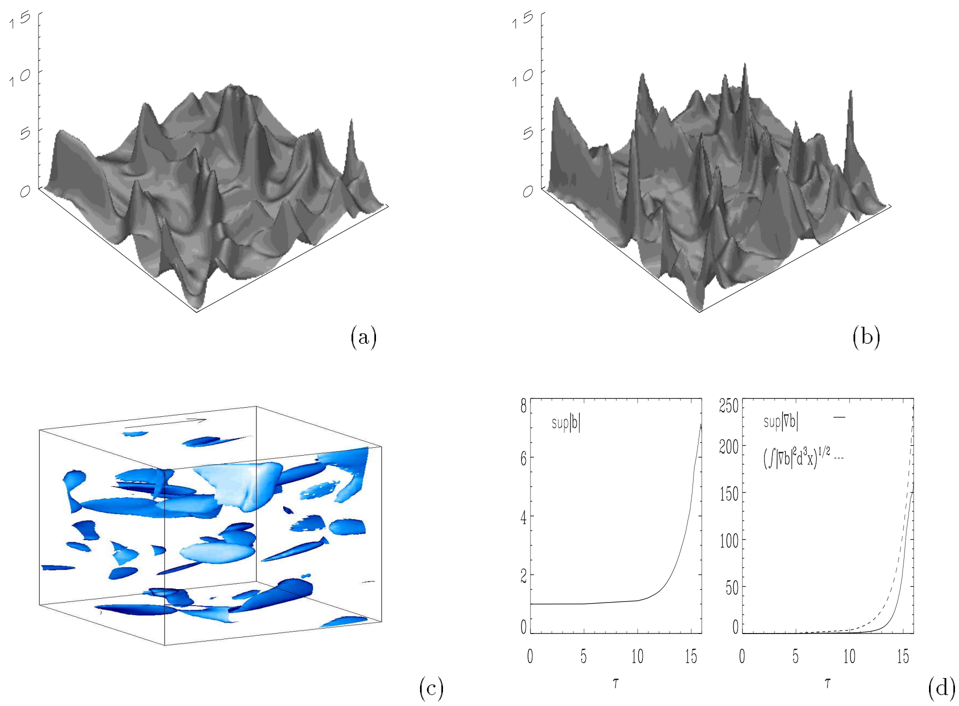

Fig. 4. Evolution of an initially circularly polarized Alfvén wave with $\beta = 3$ and $\nu = 0.5$: snapshot of $|b|^2$ in a plane transverse to the ambient field at $t = 14.1$ (a) and $t = 14.7$ (b); isosurfaces $|b|^2 = 4$ (the arrow indicating the direction of the ambient field) at $t = 14.1$ (c) ; time variation of the maxima of the field $\sup|b|$ (d, left) and of the gradient norms $\sup|\nabla b|$, $\left(\int |\nabla b|^2 d^3\mathbf{x}\right)^{1/2}$ where ∇b holds for the transverse gradient matrix (d, right).

the maximum wave intensity was amplified by a factor 100 and the resolution 32×256^2 we used becomes insufficient to describe the further evolution. A three-dimensional view of the regions of high wave intensity displays quasi-circular "magnetic filaments"that are parallel to the ambient field and extend in the entire domain (Fig. 3b). It is remarkable that no significant dynamics has developed in the longitudinal direction and the quasi-monochromatic character of the wave is preserved. The circular polarization of the dominant longitudinal mode is also well maintained and the transverse dynamics accurately described by the two-dimensional NLS equation for the wave amplitude [17].

Figures 4a and 4b show at two successive times the wave intensity $|b|^2$ in a transverse plane for $\nu = 0.5$, in a run with a resolution 32×128^2 (a similar evolution was also obtained for $\nu = 3.2$). It is noticeable that although strong gradients are created, the wave intensity remains moderate. We observe the formation of magnetic layers that are parallel to the local transverse magnetic field, with a thickness that decreases in time. Inside these layers, local maxima develop with an amplitude that grows moderately. The initial circular polarization of the carrying mode $k = 1$ is observed to be progressively lost as time

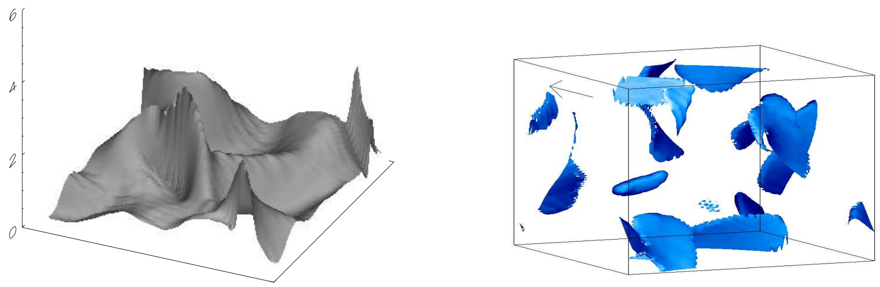

(a) (b)

Fig. 5. Snapshot of $|b|^2$ in a plane transverse to the ambient field (a) and isosurfaces $|b|^2 = 2$ (the arrow indicating the direction of the ambient field) (b), for an initially circularly polarized Alfvén wave with $\beta = 3$ and $\nu = 0.01$ at $t = 23$.

elapses. Furthermore, the growth of the transverse gradients results in a progressive amplification of the second longitudinal harmonics whose amplitude at the end of the simulation is in a ratio of only a few units with that of the mode $k = 1$. The longitudinal dynamics is conspicuous on Fig. 4c that displays the formation of "magnetic pancakes" of finite extension in the direction of the ambient field. Similar magnetic pancakes, with superimposed small random structures, are obtained in a simulation with $k = 1$ and a broad-spectrum isotropic initial noise (not shown).

Figure 4d compares the amplification in time of the supremum of the wave amplitude and of its gradients (in both local and integrated norms). It suggests a possible finite-time blowup of the transverse gradients, while the maximum value of the amplitude remains finite and increases with ν. A detailed analysis of these issues would require simulations at much higher resolutions than those presently available.

Finally, Fig. 5a shows the regime that develops for $\nu = 0.01$ in a simulation at resolution 64^3. In this case, the amplitude is only weakly amplified. Fronts develop in the transverse directions, but the peaks visible for $\nu = 0.5$ (Fig. 4b) are no longer present. Furthermore, a significant steepening is now visible in the longitudinal direction. The spectrum in this direction indeed becomes more populated at small scales, although the carrier mode remains dominant. A three-dimensional visualization of the resulting magnetic structures is displayed in Fig. 5b.

2.2 A simple envelope-model

The above simulations with initial conditions in the form of a perturbed Ferraro wave show that even when the dynamics is not strongly dispersive and thus not amenable to a classical NLS modulation analysis, the transverse dynamics is dominant, at least at early enough times. This suggests a simple amplitude description retaining only one longitudinal wavenumber. We nevertheless permit the development of the other polarization and do not prescribe any scale separation at the level of the time variable. We thus write

$$b = \psi_+^*(\eta, \zeta, \tau)e^{-i\theta_+} + \psi_-(\eta, \zeta, \tau)e^{i\theta_-}, \tag{9}$$

where $\theta_\pm = k\xi - \omega_\pm \tau$ and $\omega_\pm = \pm\frac{k^2}{2R_i}$, ψ_+^* and ψ_- being the amplitudes of the right and the left-polarized modes respectively.

Defining $\partial_\pm = \partial_\eta \pm i\partial_\zeta$ (previously denoted by $\partial_\perp$ and $\partial_\perp^*$), the divergenceless condition (8) gives

$$\widetilde{b}_x = \frac{i}{2k}\left(\partial_+\psi_+ e^{i\theta_+} + \partial_-\psi_- e^{i\theta_-}\right) + \text{c.c.}, \tag{10}$$

while the pressure P reads

$$P = \frac{1}{2(1-\beta)}\left(\frac{i}{k}(\partial_+\psi_+ e^{i\theta_+} + \partial_-\psi_- e^{i\theta_-}) + \psi_+\psi_- e^{i(\theta_+ + \theta_-)}\right) + \text{c.c.} \tag{11}$$

By projecting eq. (6) on the spatial Fourier modes $e^{ik\xi}$ and $e^{-ik\xi}$, one obtains

$$i\partial_\tau\psi_\pm + k\Big(\frac{|\psi_\mp|^2}{4(\beta-1)} - \bar{u}_x - \frac{\bar{b}_x}{2}\Big)\psi_\pm - \frac{1}{4k(\beta-1)}\Big(\Delta\psi_\pm + \alpha_\pm\partial_\mp^2\psi_\mp\Big) = 0 \tag{12}$$

that contains the functions of time $\alpha_\pm(\tau) = e^{\pm i(\omega_+ - \omega_-)\tau} = e^{\pm\frac{ik^2}{R_i}\tau}$.

The mean field $\bar{u}_x$ can be eliminated by deriving from eq. (12) the relation

$$\partial_\tau\Big(|\psi_+|^2 + |\psi_-|^2\Big) = \frac{i}{4k(\beta-1)}\Big(\psi_+\Delta\psi_+^* + \psi_-\Delta\psi_-^* - \alpha_+\psi_+^*\partial_-^2\psi_- - \alpha_-\psi_-^*\partial_+^2\psi_+\Big) + \text{c.c} \tag{13}$$

where $\Delta = \partial_+\partial_-$ is the transverse laplacian.

Combining eq. (13) with eq. (7), one gets $\bar{u}_x = |\psi_+|^2 + |\psi_-|^2$. Moreover, after projection, one has $\bar{b}_x = -\frac{1}{1+\beta}(|\psi_+|^2 + |\psi_-|^2)$ when dropping the constant E_M that plays no dynamical role. One finally obtains that in eqs. (12)

$$\bar{u}_x + \frac{\bar{b}_x}{2} = \frac{4\beta+3}{4(1+\beta)}\Big(|\psi_+|^2 + |\psi_-|^2\Big). \tag{14}$$

In the strong dispersion limit $\nu \to \infty$, the time scale of the transverse dynamics is much longer than the period of the carrier and averaging over the fast oscillations leads to take $\alpha_\pm = 0$ in the above amplitude equations. In this case, eq. (12) can also be derived by a standard weakly nonlinear modulation analysis retaining both right-hand and left-hand polarized modes.

When ν takes a finite value, the time-dependent factors $\alpha_\pm$ in eq. (12) are to be retained. They can however be formally eliminated by absorbing them in a redefinition of the amplitudes. One then recovers the equations for the fields B_-, B_+ given in ref. [21] where the analysis is based on a modulational approach, assuming values of the parameter ν that are large enough for the dynamics to be mostly monochromatic in the longitudinal direction but not sufficient to enforce circular polarization. For this purpose, depending on the choice $\sigma = 1$ or $\sigma = -1$ of the initial polarization, one writes either $B_- = \alpha_- \psi_+$ and $B_+ = \psi_-$ or $B_+ = \alpha_+ \psi_-$ and $B_- = \psi_+$.

By defining the vector $\mathbf{B} = (0, \frac{1}{2}(B_- + B_+), \frac{i}{2}(B_- - B_+))$, one then recovers the vector NLS equation [2] (37) of ref. [21]

$$
\begin{aligned}
i\partial_\tau \mathbf{B} + \frac{k^2}{2R_i}(\sigma\mathbf{B} + i\mathbf{B}\times\mathbf{e}_1) - \frac{1}{2k(\beta-1)}\nabla(\nabla\cdot\mathbf{B}) \\
+\frac{k(8\beta^2 - 3\beta - 7)}{4(1+\beta)(1-\beta)}|\mathbf{B}|^2\mathbf{B} - \frac{k}{4(\beta-1)}\mathbf{B}\times(\mathbf{B}\times\mathbf{B}^*) = 0,
\end{aligned} \tag{15}
$$

where $\mathbf{e}_1$ is the unit vector in the direction of the ambient field.

The numerical integrations of eq. (15) reported in [21] display a qualitative agreement with the simulations of the 3D-DNLS equations presented in Sec. 2.1. Although the amplitude model does not retain the longitudinal structure that develops for small or moderate values of ν, it does suggest a blowup of the gradients and the growth of the amplitude maximum to a moderate value that increases with ν. The transverse configuration of the magnetic structures is also very similar to that described in the present paper, with a progressive transition towards the usual NLS foci as ν is increased.

The success of the amplitude equations for moderate ν in the context of the present simulations is probably due to the fact that Ferraro waves are exact solutions of the one-dimensional problem. As a consequence, longitudinal harmonics develop on a time scale comparable to that of the onset of a strong transverse dynamics, making the projection method acceptable for a simplified description of the transverse modulation of a Ferraro wave.

[2] Reference [21] contains a misprint in the coefficient in front of $|\mathbf{B}|^2\mathbf{B}$.

Equation (15) admits an Hamiltonian $\mathcal{H}$ [21], that satisfies the inequality $p\int |\nabla \cdot \mathbf{B}| d\mathbf{x}_\perp \leq |\mathcal{H}| + q(\sup|B|)^2 + r$ where, for finite ν, the quantities p, q, r are positive and depend on the initial conditions. As a consequence, moderate values of $\sup|B|$ implies that $|\nabla \cdot \mathbf{B}|$ remains bounded, which is consistent with the numerical observation that the transverse magnetic field is roughly parallel to the magnetic layers. In contrast, the full gradients become large.

3 Evolution of a perturbed linearly polarized wave

In the framework of the 3D-DNLS equations, initial conditions more general than a perturbed circularly polarized wave can be considered. In particular, it is possible to study the evolution of an initially linearly polarized monochromatic wave, resulting from the superposition of two Ferraro waves. Since it is not an exact solutions of the 3D-DNLS equations even in the absence of transverse perturbations, cubic couplings are now relevant. As a consequence, a significant longitudinal dynamics rapidly develops making the one-mode projection inaccurate, except in the limit $\nu \to \infty$ where the carrier harmonics are not resonant. In the latter case, the coupling of the two counter-polarized waves can be accurately described by eq. (12) with $\alpha = 0$ for which the existence of (localized) solutions that blow up in a finite time can be established by extending to this case the usual virial identity of the two-dimensional NLS equation [25]. Numerical simulations for $\nu = 50$ indeed show a dynamics very similar to that observed in the case of a circularly polarized wave, with the formation of axisymmetric filaments of strong intensity, longitudinally modulated by the interference of the two polarization modes. In contrast, simulations for $\nu = 0.5$ reveal the early formation of non-isotropic structures for the wave intensity in the transverse planes (Fig. 6a), followed by a sudden amplification of localized and more isotropic structures (Fig. 6b), a phenomenon that is not observed with initially circularly polarized waves. This effect could result from the rapid generation of higher-wavenumber longitudinal harmonics, leading to an enhancement of the dispersion compared with the nonlinearity and to a larger effective ν, more favorable for amplitude blowup.

4 Dynamics of an initial wave packet

In most realistic situations, Alfvén waves are not quasi-monochromatic and the question arises of the evolution of a weakly-nonlinear dispersive wave with a broad spectrum. To investigate this issue, we numerically integrated the 3D-DNLS equations for $\nu = 50$ with initial conditions in the form of transversally perturbed packets of right-hand circularly polarized waves with a gaussian

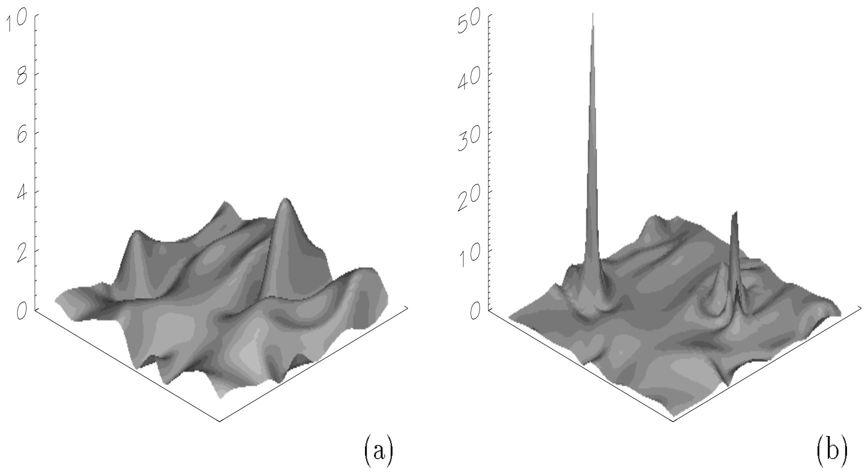

Fig. 6. Snapshot of $|b|^2$ in a plane transverse to the ambient field for an initially linearly polarized Alfvén wave with $\beta = 3$ and $\nu = 0.5$, at $t = 17.2$ (a) and $t = 18.8$ (b).

spectrum of the form $|b_k|^2 = \frac{b_0^2}{\delta\sqrt{2\pi}} e^{-\frac{(k+1)^2}{2\delta^2}}$. For a given resolution, such a spectrum requires a computational box with a longer size L_x in the longitudinal direction. When the spectrum is very narrow, the wave packet keeps its identity before developing a transverse collapse, leading to the formation of intense magnetic structures with a spindle shape. Differently, for left-hand polarization the early evolution of a narrow wave packet corresponds to a longitudinal defocusing, as expected from the amplitude equations (2.30)–(2.33) of ref. [17] taken in the long-wavelength limit. When the mean longitudinal fields become relevant, transverse focusing develops.

Figures 7a and 7b refer respectively to simulations of a right-hand polarized wave packet with $\delta = 0.09$ (in a box of size $(12\pi) \times (2\pi)^2$) and $\delta = 0.2$ (in a box of size $(32\pi) \times (2\pi)^2$). In both cases, the wave packet first disperses and looses its shape, but the non-monochromatic character of the wave does not prevent a subsequent transverse self-focusing in spite of an important longitudinal dynamics. With the former parameters, the development of three-dimensional magnetic structures in the form of modulated tubes is observed, while for the broader wave packet they rather take the form of chains of "magnetic bubbles". Finally, a simulation with $\delta = 1$ displays a complex longitudinal dynamics before the development of the transverse instability that leads to a violent collapse in localized regions of the x-axis. The resulting structures appear to be sparse and randomly distributed three-dimensional objects.

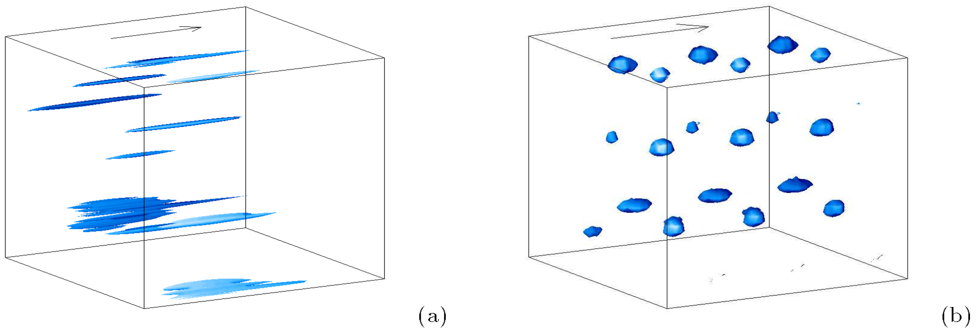

Fig. 7. Isosurfaces $|b|^2 = 15$ for an initial wavepacket (the arrow indicating the direction of the ambient field) with $\beta = 3$ and $\nu = 50$, for $L_x = 12\pi$, $\delta = 0.09$ (a) and $L_x = 32\pi$, $\delta = 0.2$ (b).

5 Conclusion

The nonlinear dynamics of long-wavelength dispersive Alfvén waves was studied in the context of the three-dimensional DNLS equation. In the strongly dispersive regime associated with small-amplitude waves, a slightly perturbed right-hand circularly polarized monochromatic wave train collapses in the transverse directions leading to strong magnetic filaments parallel to the ambient field, as asymptotically described by the two-dimensional NLS equation. A similar dynamics was obtained for left-hand or linear polarizations under the condition that the initial noise be concentrated on wavenumbers close enough to that of the pump to prevent the development of small-scale oblique instabilities. When the effect of the dispersion is reduced (larger wave amplitude), numerical simulations show that the wave amplitude is only moderately amplified, while strong gradients still develop. Pancake-like magnetic structures are created, corresponding to the formation of thin magnetic layers in the transverse planes and the development of harmonics in the longitudinal direction. When the dispersion becomes small compared with the nonlinear effects, a strong longitudinal dynamics takes place while magnetic fronts are formed in the transverse planes. This regime deserves further investigations, especially when dissipative processes are included in eq. (6), leading to a three-dimensional extension of the Cohen-Kulsrud-Burgers equations [26], [27]. We also show that the transverse focusing of weakly-nonlinear dispersive waves is robust when the spectrum of the initial conditions is broadened. It is remarkable that despite the existence of a non-trivial longitudinal dynamics, a transverse collapse takes place, resulting in three-dimensional structures of intense magnetic field.

The strong growth of the transverse gradients implies a breakdown of the asymptotics leading to the 3D-DNLS equations that assumes slower variations in the transverse directions than in the longitudinal one. It is then necessary to go back to the primitive MHD equations which involve a more complex dynamics including couplings to the magneto-sonic waves and to backward-propagating waves. Preliminary direct numerical simulations of the three-dimensional Hall-MHD equations, not restricted to the long-wavelength regime, are presented in [28] where various nonlinear evolutions are obtained depending on the competition between the different linear instabilities. The question also arises whether finite-time singularities occur on the primitive equations or whether the violent amplification effects displayed by the 3D-DNLS equations saturate at a finite value.

We conclude by mentioning the role of the kinetic effects that are believed to be relevant when the parameter β exceeds unity. In one space dimension, they were modeled at the level of the long-wave asymptotics by additional nonlocal terms in the DNLS equation [10], [2], [29]. Extension of this description to higher dimensions is in project.

Acknowledgments

Computations were performed on the CRAY94 and CRAY98 machines of the Institut du Développement et des Ressources en Informatique Scientifique and on the facilities of the Program "Simulations Interactives et Visualisation en Astronomie et Mécanique (SIVAM)". This work was supported in part by "Programme National Soleil Terre" of CNRS and by INTAS grant No. 96-0413.

References

[1] Huba, J.D., Phys. Plasmas **2**, 2504 (1995).

[2] Spangler, S.R., Phys. Fluids B **2**, 407 (1990).

[3] Spangler, S., Fuselier, S., Fey, A. and Anderson, G., J. Geophys. Res. **93**, No A2, 845 (1988).

[4] Rogister, A., Phys. Fluids **14**, 2733 (1971).

[5] K. Mio, T. Ogino, K. Minami and S. Takeda, Phys. Soc. Japan **41**, 265 (1975).

[6] E. Mjølhus, J. Plasma Phys. **16**, 321 (1976).

[7] C.F. Kennel, B. Buti, T. Hada and R. Pellat, Phys. Fluids **31**, 1949 (1988).

[8] Mjølhus, E. and Hada, T. in *Nonlinear Waves and Chaos in Space Plasmas*, T. Hada and H. Matsumoto eds., 121, Terra Scientific Publishing Company, Tokyo (1997).

[9] Kaup, D.J and Newell, A.C., J. Math. Phys., **19**, 798 (1978).

[10] Mjølhus, E. and Wyller, J., J. Plasma Phys. **40**, 299 (1988).

[11] Passot, T. and Sulem, P.L., Phys. Rev. E **48**, 2966 (1993).

[12] Gazol, A., Passot, T., and Sulem, P.L., Phys. Plasmas, **6**, 3114 (1999).

[13] Viñas, A.F. and Goldstein, M.L., J. Plasma Phys., **46**, 107; 129 (1991).

[14] Spangler, S.R., in *Nonlinear Waves and Chaos in Space Plasmas*, T. Hada and H. Matsumoto eds., 171, Terra Scientific Publishing Company, Tokyo (1997).

[15] Champeaux, S., Laveder, D., Passot, T., and Sulem, P.L., Nonlin. Proces. Geophys. **6**, 169 (1999).

[16] Shukla, P.K. and Stenflo, L., Space Sci., **155**, 145 (1989).

[17] Champeaux, S., Passot, T., and Sulem, P.L., J. Plasma Phys., **58**, 665 (1997).

[18] Sulem, C. and Sulem, P.L., *The Nonlinear Schrödinger Equation: Self-Focusing and Wave Collapse*, Applied Mathematical Sciences **139**, Springer-Verlag (1999).

[19] Zakharov, V.E., in *Handbook of plasma physics*, M.N. Rosenbluth and R.Z. Sagdeev, eds., vol. 2 (A.A. Galeev and R.N. Sudan, eds.), 81, Elsevier (1984).

[20] Ferraro, V.C.A., Proc. R. Soc. London Ser A **233**, 310 (1955).

[21] Champeaux, S, Passot, T., and Sulem, P.L., Phys. Plasmas **5**, 100 (1998).

[22] Champeaux, S., Gazol, A., Passot, T., and Sulem, P.L., in *Nonlinear MHD Waves and Turbulence*, T. Passot and P.L. Sulem eds., Lecture Notes in Physics **536**, 54, Springer-Verlag (1999).

[23] Whitham, G.B., *Linear and Nonlinear Waves*, Wiley (1974).

[24] Luke, J.C., Proc. Roy. Soc. London A **292**, 403 (1966).

[25] McKinstrie, C.J. and Russel, D.A., Phys. Rev. Lett. **61**, 2929 (1988).

[26] Cohen, R. and Kulsrud, R., Phys. Fluids **17**, 2215 (1974).

[27] Wu, C.C. and Kennel, C.F., Phys. Rev. Lett. **68**, 65 (1992).

[28] Laveder, D., Passot, T., and Sulem, P.L., "Instabilities and filamentation of dispersive Alfvén waves", Proc. 4^{th} UNAM Supercomputing Conference (Mexico City, June 2000), World Scientific, to appear.

[29] Medvedev, M. V. and Diamond, P. H., Phys. Plasmas **3**, 863 (1995).

Figure captions

Figure 1: Spectral instability range as delimited by the contours of Fourier modes of b_y obtained by two-dimensional numerical simulations of the 3D-DNLS equations, for initially right-hand (a) and left-hand (b) circularly polarized Alfvén waves with $\beta = 2$ and $\nu = 50$. The mode $k_x = 1$, $k_y = 0$ corresponds to the pump wave. At the resolution of Fig. 1a, the longitudinal instability is not visible.

Figure 2: Isosurfaces $|b|^2 = 20$ for an initially right-hand polarized Alfvén wave (a), and $|b|^2 = 3$ for a left-hand polarized Alfvén wave (b), when $\beta = 2$ and $\nu = 50$. The arrow indicates the direction of the ambient field.

Figure 3: Snapshot of $|b|^2$ in a plane transverse to the ambient field (a) and isosurfaces $|b|^2 = 10$ (the arrow indicating the direction of the ambient field) (b), for an initially circularly polarized Alfvén wave with $\beta = 3$ and $\nu = 50$ at $t = 9.8$.

Figure 4: Evolution of an initially circularly polarized Alfvén wave with $\beta = 3$ and $\nu = 0.5$: snapshot of $|b|^2$ in a plane transverse to the ambient field at $t = 14.1$ (a) and $t = 14.7$ (b); three-dimensional isosurfaces $|b|^2 = 4$ (the arrow indicating the direction of the ambient field) at $t = 14.1$ (c) ; time variation of the maxima of the field $\sup|b|$ (d, left) and of the gradient norms $\sup|\nabla b|$, $\left(\int |\nabla b|^2 d^3\mathbf{x}\right)^{1/2}$ where ∇b holds for the transverse gradient matrix (d, right).

Figure 5: Snapshot of $|b|^2$ in a plane transverse to the ambient field (a) and isosurfaces $|b|^2 = 2$ (the arrow indicating the direction of the ambient field) (b), for an initially circularly polarized Alfvén wave with $\beta = 3$ and $\nu = 0.01$ at $t = 23$.

Figure 6: Snapshot of $|b|^2$ in a plane transverse to the ambient field for an initially linearly polarized Alfvén wave with $\beta = 3$ and $\nu = 0.5$, at $t = 17.2$ (a) and $t = 18.8$ (b).

Figure 7: Isosurfaces $|b|^2 = 15$ for an initial wavepacket (the arrow indicating the direction of the ambient field) with $\beta = 3$ and $\nu = 50$, for $L_x = 12\pi$, $\delta = 0.09$ (a) and $L_x = 32\pi$, $\delta = 0.2$ (b).